Journal of Heat Transfer

Technical Note

Weakly Ionized Plasma Arc Heat Transfer Between Geometrically Dissimilar Electrodes

S. S. Sripada,[1] P. S. Ayyaswamy,[1] and I. M. Cohen[1]

A set of self-consistent conservation equations for the charged particle densities and the temperatures in a weakly ionized plasma between two dissimilar electrodes is numerically solved using an orthogonal body-fitted coordinate system. The electron number density and temperature variation in the discharge gap, and the results for the heat transfer to the anode are presented. Results have been developed for a configuration that commonly arises in microelectronic manufacturing—a thin cylindrical anode together with a planar cathode.

Nomenclature

A_i, B_i = constants in expression for ionization coefficient
a = accommodation coefficient
d = anode diameter
E = magnitude of electric field intensity
$\mathbf{E}$ = electric field intensity vector
e = electron charge
g = statistical weight
h = Planck's constant
I = current
$\mathbf{j}$ = species number flux
k = Boltzmann constant
l = length
m = mass
N = species number density
$\mathbf{n}$ = surface normal vector
P_i = ionization rate due to electron impact
P_t = thermal ionization rate
p = pressure
$\mathbf{q}$ = energy flux
(r, z) = cylindrical coordinates
$\mathbf{R}$ = position vector
R_c = external circuit resistance
R_t = three-body recombination rate
T = temperature (K)
V = electric potential

Greek Symbols

α_i = primary ionization coefficient
ϵ_0 = permittivity of free space
γ = three-body recombination coefficient
κ = thermal conductivity
μ = mobility
ϕ = work function
(ξ, η) = computational grid system

Subscripts

an = anode
ap = applied
c = conductive
d = discharge
e = electron
g = inter-electrode gap
i = ion, ionization
m = melting
n = neutral specie, surface normal
p = cathode plate
ref = reference
∞ = ambient

Superscripts

$*$ = nondimensional

Introduction

In many manufacturing processes, arc plasma heat transfer occurs between two dissimilar electrodes. High energy plasmas occur in such applications as arc welding and plasma spray coating. On the other hand, low energy plasmas are used in plasma processing in the microelectronics industry. Since electrode geometry significantly affects the electric field and the plasma transport, it is important to be able to correctly evaluate the heat transfer in such situations taking into account the geometrical variations. In this context, Jog et al. (1991, 1992) have studied the initial breakdown of the inter-electrode gap and the heat transfer to the tip of a wire in a wire-to-plane discharge. Qin (1997) numerically simulated the glow discharge between two dissimilar electrodes, a cylindrical anode and a planar cathode using a nonorthogonal body-fitted coordinate system based on elliptic grid generation (Knupp and Steinberg, 1993). The use of a nonorthogonal grid system, however, introduces cross-derivative terms which considerably complicate the numerical solution with attendant convergence difficulties. In this study, we have examined plasma arc heat transfer between two dissimilar electrodes taking into account Poisson's equation for the self-consistent electric potential. A set of continuum conservation equations for the charged particle densities and the heat

[1] Department of Mechanical Engineering and Applied Mechanics, University of Pennsylvania, Philadelphia, PA 19104-6315.

Contributed by the Heat Transfer Division for publication in the JOURNAL OF HEAT TRANSFER. Manuscript received by the Heat Transfer Division, Sept. 30, 1997; revision received, Sept. 15, 1998. Keywords: Heat Transfer, Melting, Phase Change, Plasma, Solidification. Associate Technical Editor: M. Modest.

fluxes in an arc plasma has been solved using an orthogonal grid system to minimize errors both grid based and those arising from approximate representations for boundary fluxes. We have presented results for a flat cathode and a spherical-tipped slender wire anode, a configuration that arises in many manufacturing processes.

Theory

A typical low-energy discharge may be characterized by a low-energy continuum description of a "weakly" ionized plasma. The plasma consists of three species: neutrals, ions (positive), and electrons. For such a continuum steady-state plasma, the governing equations are as follows. The number conservation equation is

$$\nabla \cdot \mathbf{j}_{e,i} = P_i(N_e) + P_t(N_e) - R_t(N_e), \tag{1}$$

where the electron and ion number fluxes are given by

$$\mathbf{j}_{e,i} = -\frac{\mu_{e,i}}{e} \nabla p_{e,i} \mp \mu_{e,i} N_{e,i} \mathbf{E}, \; p_{e,i} = N_{e,i} k T_{e,i}. \tag{2}$$

The electron energy equation is

$$\nabla \cdot \mathbf{q}_e = -e\mathbf{j}_e \cdot \mathbf{E}, \quad \text{where} \quad \mathbf{q}_e = \tfrac{5}{2} k T_e \mathbf{j}_e - \kappa_e \nabla T_e. \tag{3}$$

The self-consistent electric field is given by Gauss' law

$$\nabla \cdot \mathbf{E} = \frac{e}{\epsilon_0}(N_i - N_e), \quad \text{where} \quad \mathbf{E} = -\nabla V. \tag{4}$$

$P_i(N_e)$ is the ionization rate due to electron impact (von Engel, 1965):

$$P_i = \alpha_i \mu_e E N_e, \text{ where } \alpha_i = A_i p \exp\left(\frac{-B_i p}{E}\right).$$

$P_t(N_e)$ is the thermal ionization rate, $R_t(N_e)$ is the three-body recombination rate. We employ the Saha equation (Mitchner and Kruger, Jr., 1973) to obtain the net ionization due to both thermal ionization and recombination,

$$P_t(N_e) - R_t(N_e) = \gamma\left[\frac{2 g_i N_n}{g_n}\left(\frac{2\pi m_e k T_e}{h^2}\right)^{3/2} \exp\left(-\frac{eV_i}{kT_e}\right) - N_e N_i\right],$$

where the three-body recombination coefficient $\gamma = 1.09 \times 10^{-20} T_e^{-(9/2)} N_e$ (m^3/s) is a strong function of electron temperature (Hinnov and Hirschberg, 1962).

The heat flux from the plasma to the electrode has two major components, the work function energy flux and the conductive energy flux. For low-energy plasmas, all other modes of energy transport are likely to be negligible compared to these two components (Jog et al., 1992; Ayyaswamy et al., 1998). Incoming electrons at the anode release energy equivalent to the work function, ϕ, to the electrode surface. The net surface normal energy flux may be expressed as $q_n = a_e e \phi \mathbf{j}_e \cdot \mathbf{n}$, where $a_e = 0.9$ is the assumed electron accommodation coefficient for the anode surface (Wiedmann and Trumpler, 1946), and $\mathbf{n}$ is the surface normal vector. The conductive heat flux from the electrons is due to their thermal energy and is expressible as $q_c = -\kappa_e \nabla T_e \cdot \mathbf{n}$.

In this study, the above set of equations is solved in the axisymmetric cylindrical coordinate (r, z) system. In such an axisymmetric framework, the center of the circular planar cathode is located at $r = z = 0$ and the cathode radius is r_p. The spherical tip of the anode is represented by a spherical segment attached to a long slender cylinder (wire) of length l_{an} oriented along the z-axis. The tip is at a distance l_g, the gap length, from the center of the cathode plate. In the numerical simulation, the physical domain is truncated at a radius equal to that of the cathode plate which is taken to be much larger than the anode diameter so that the effect of the domain size on the transport to the anode is negligible. The boundary of the domain thus consists of the anode and its tip, the axis of symmetry, the cathode plate, and the outer periphery connecting the end of the anode to the outer edge of the cathode plate.

The boundary conditions may be stated as follows.

At the cathode plate $(0 \le r \le r_p, z = 0)$

$$N_{e,i} = N_0, \quad V = V_{ap} - I_{an} R_c, \quad T_e = T_\infty.$$

At the anode tip and on the lateral surface

$$N_{e,i} = N_0, \quad V = 0, \quad T_e = T_s.$$

At the axis of symmetry $(r = 0, 0 \le z \le l_g)$

$$\frac{\partial N_{e,i}}{\partial r} = 0, \quad \frac{\partial V}{\partial r} = 0, \quad \frac{\partial T_e}{\partial r} = 0.$$

At the outer boundary

$$N_{e,i} = N_0, \quad \nabla V \cdot \mathbf{n} = 0, \quad \nabla T_e \cdot \mathbf{n} = 0.$$

Here, N_0 is the small ambient electron and ion density due to omnipresent background radiation. We consider the electrodes to be nearly perfect absorbing surfaces for the ionic species. The spherical tip of the anode is assumed to be at a constant prescribed temperature T_m, and the surface temperature T_s is assumed to decrease linearly along its axis beyond the spherical tip. I_{an} is the current collected at the anode and is expressed as

$$I_{an} = e \int_{anode} (\mathbf{j}_i - \mathbf{j}_e) \cdot d\mathbf{A}_{an}$$

where the integral is taken over the entire surface of the anode and $d\mathbf{A}_{an}$ is the elemental area vector.

The governing equations are nondimensionalized by the anode diameter d as the length scale, $\mu_e k T_\infty/(ed)$ as the velocity scale, kT_∞/e as the voltage scale, and the ambient temperature T_∞ as the temperature scale. The number densities have been nondimensionalized by the density N_{ref} that results in a Debye length equal to the chosen length scale d, that is, $N_{ref} = \epsilon_0(kT_\infty/e^2 d^2)$. Next, we describe the numerical procedures adopted to solve the dimensionless equations.

Numerical Methodology

The chosen domain is irregular in that two of the four domain boundaries, the anode and the outer boundary, do not coincide with either of the (r, z) coordinate lines. We have generated a 41×41 *orthogonal* structured grid based on the solution of highly nonlinear coupled covariant Laplace equations (Ryskin and Leal, 1983; Eca, 1996) with the prescribed domain coordinates as boundary conditions. The finite volume method was used to discretize these equations, and an iterative algorithm is used for solution.

Since the arc heat transfer problem is axisymmetric but the (ξ, η) grid system is two-dimensional, the governing equations for the plasma are first written in the (r, z) coordinate system and *then* transformed to the computational (ξ, η) domain. A finite volume method was used in conjunction with the power-law scheme (Patankar, 1980) to discretize the partial differential equations.

A novel interpretation of the power-law scheme was necessary for use with the plasma equations. In the equations, the electric field, $\mathbf{E}$, plays the role of a convection "velocity" in the fluid dynamics sense. Therefore the ratio, $e\mathbf{E} \cdot \mathbf{t}_\zeta \Delta\zeta/kT_e$, the "electronic Peclet" number is used in lieu of the standard grid Peclet number. Here $\mathbf{t}_\zeta$ is the local tangent vector to the ζ

coordinate line where ζ may be either of (ξ, η) as appropriate. All dependent variables are colocated at the grid points.

The discretized equations are strongly nonlinear and coupled and were solved iteratively with severe under-relaxation. Due to the disparate velocity scales for the ions and electrons (electrons are orders of magnitude more mobile than ions, $\mu_e/\mu_i \sim 200$), relaxation parameters for the equations had to be suitably tailored to obtain a convergent solution. This required extensive numerical experimentation.

Numerical error in the simulation may stem from (i) grid generation, (ii) plasma equations discretization, (iii) the iterative solver, and (iv) machine error. Grid generation error from discretization and departure from orthogonality are $\sim 10^{-4}$ and ± 0.94 percent, respectively. Plasma equations discretization error is $\sim 10^{-4}$. The sensitivity of the solutions to grid coarseness was tested by performing the simulations on a variety of grids. The coarsest grid (21×21) failed to capture the sheath region satisfactorily. Using the finest grid, 61×61, changed the solutions by a maximum of 1.02 percent relative to the 41×41 grid.

The simulations were performed on a CRAY C90 at the Pittsburgh Supercomputing Center.

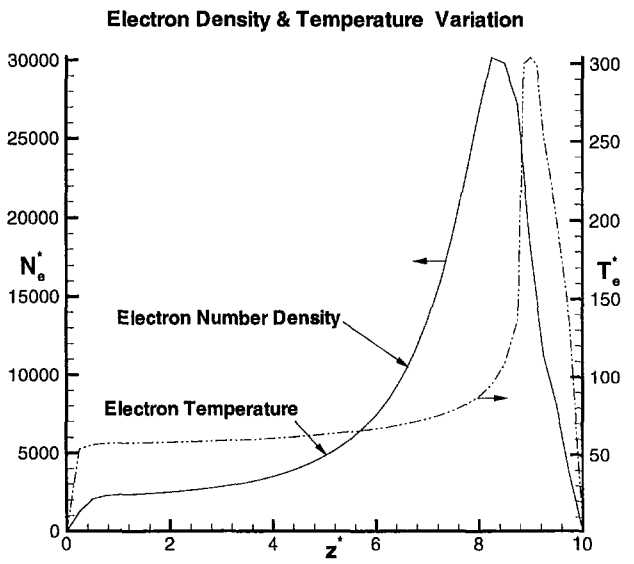

Fig. 1 Variation of normalized electron density and temperature along discharge axis

Results and Discussion

Numerical simulations were made for air as the medium with all the input parameters specified. The chosen values are typical of an EFO discharge used in the microelectronic industry. The parameters are: an applied voltage of -3000 V, an anode (wire) diameter $d = 1$ mil $= 25.4$ μm, a discharge gap $l_g = 10d$, an anode length $l_{an} = 30d$ from the anode tip, and the cathode plate radius $r_p = 40d$. The melting temperature of the anode material was prescribed to be $T_m = 1336$ K (this corresponds to a gold anode which is often used in microelectronic applications). The ambient reference temperature is $T_\infty = 300$ K, and the ambient pressure is 1 atmosphere which together specify the number density of neutrals $N_n = 2.44 \times 10^{25}$ m^{-3}. The small ambient ion density due to background radiation is taken to be $N_0 = 6 \times 10^8$ m^{-3}. The mobilities are $\mu_e = 3.48 \times 10^{-2}$ m^2(Vs)$^{-1}$ and $\mu_i = 1.7 \times 10^{-4}$ m^2 (Vs)$^{-1}$. These parameters result in a reference number density $N_{ref} = 2.22 \times 10^{15}$ m^{-3} and a reference voltage $V_{ref} = kT_\infty/e = 2.5875 \times 10^{-2}$ V. The ionization potential is taken to be 14.87 V. The outer circuit resistance was taken to be $R_c = 100$ kΩ. In the results presented in the following, all lengths (r, z) are nondimensionalized by d.

In Fig. 1 we present the variation of the nondimensional electron number density $N_e^* = N_e/N_{ref}$ along the discharge axis with the cathode at $z^* = 0$ and anode tip at $z^* = 10$. Due to the strong potential gradients near the anode surface the electric field intensity is high and impact ionization becomes a strong ionization source as electrons accelerate to large drift velocities near the anode. Thus there is a peak in the electron density near the anode. However, the strongly absorbing electrode boundary condition causes a severe gradient in the density at the anode. Since ions are generated at the same locations as electrons, an identical trend is seen for ions except for differences in gradients in the thin electrode sheaths.

In Fig. 1 we present the electron temperature variation along the symmetry axis. Due to the strong potential gradient at the anode, electrons undergo much stronger acceleration and thus assume large kinetic energies which is in turn reflected in the temperature. At the anode a constant temperature is prescribed which also acts as a strong energy-absorbing boundary condition. This is reflected in the temperature peak in the anode vicinity and the strong gradient. The gradient results in a large heat flux to the anode surface. As one moves away from the axis along the anode surface, the temperature gradient decreases in magnitude resulting in a decreasing heat flux. This is reflected in Fig. 2 where the variation of q^*, the dimensionless heat flux, with distance along the anode surface from the tip, is shown.

The heat flux is rendered dimensionless by $q_{ref} = kT_\infty(\mu_e N_{ref} V_{ref}/d)$ which is 3.2582×10^{-4} W/m^2 for the parameters considered. The minimum in the logarithmic heat flux variation appears at the "neck" of the anode where the segment of sphere is attached to the cylindrical portion of the anode. Beyond the spherical tip, there is enough ionization in the sheath to provide an energy flux to the anode surface albeit orders of magnitude lower than that in the vicinity of the tip. Moreover, it may be recalled that the anode surface temperature is assumed to decrease linearly along the anode axis beyond the spherical tip. For the chosen set of parameters, 0.104 W of thermal power is transferred to the anode from the plasma. Here, the bulge of the spherical tip acts like a shield against all energy driving gradients and explains the heat flux minimum. This is a novel result and indicates the crucial role played by electrode geometry in the determination of the heat flux from an arc plasma.

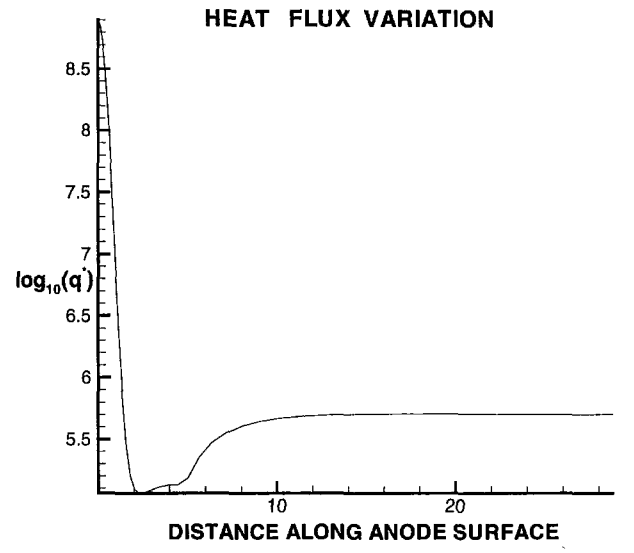

Fig. 2 Variation of nondimensional heat flux along anode surface

Conclusions

A numerical study of the heat transfer from a weakly ionized plasma between geometrically dissimilar electrodes that occurs in many manufacturing situations, and in particular in the microelectronics industry, has been described. An orthogonal body-fitted uniform grid system was generated to accurately model the plasma equations including geometrical variations in the domain. Results for the number densities, temperature, and heat flux were presented. A novel result of a minimum in the heat flux at the neck of the anode for the chosen electrode shape has also been presented.

Acknowledgments

The authors gratefully acknowledge support of this work by the National Science Foundation through NSF Grant CTS-94-21598, the Pittsburgh Supercomputing Center through Grant DMC890001P for use of the CRAY C90. and the University of Pennsylvania Research Foundation through grant of an IBM RS/6000 workstation on which much of the code development was undertaken. We also thank Prof. M. A. Jog, Department of Mechanical, Industrial, and Nuclear Engineering, University of Cincinnati, Cincinnati, OH, for stimulating discussions of some of the numerical methodology used in this study.

References

Ayyaswamy, P. S., Sripada, S. S., and Cohen, I. M., 1998, "Interfacial motion of a molten layer subject to plasma heating," *Fluid Dynamics at Interfaces,* W. Shyy, Cambridge University Press, New York, in press.

Eca, L., 1996, "2D orthogonal grid generation with boundary point distribution control," *J. Comp. Phys.,* Vol. 125, pp. 440–453.

Hinnov, E., and Hirschberg, J. G., 1962, "Electron-ion Recombination in Dense Plasmas," *Phys. Rev.,* Vol. 125, No. 3, pp. 795–801.

Jog, M. A., Cohen, I. M., and Ayyaswamy, P. S., 1991, "Breakdown of a Wire-to-plane Discharge," *Phys. Fluids B,* Vol. 3, pp. 3532–3536.

Jog, M. A., Cohen, I. M., and Ayyaswamy, P. S., 1992, "Electrode Heating in a Wire-to-plane Arc," *Phys. Fluids B,* Vol. 4, pp. 465–472.

Knupp, P., and Steinberg, S., 1993, *Fundamentals of Grid Generation,* CRC Press, Boca Raton, FL.

Mitchner, M., and Kruger, Jr., C. H., 1973, *Partially Ionized Gases,* John Wiley and Sons, New York.

Patankar, S. V., 1980, *Numerical Heat Transfer and Fluid Flow,* Hemisphere, Washington, DC.

Qin, W., 1997, "Numerical and Experimental Studies of Heat Transfer Phenomena in Microelectronic Packaging," Ph.D. thesis, University of Pennsylvania, Philadelphia, PA.

Ryskin, G., and Leal, L. G., 1983, "Orthogonal Mapping," *J. Comp. Phys.,* Vol. 50, pp. 71–100.

von Engel, A., 1965, *Ionized Gases,* 2nd Ed., Oxford University Press, London.

Wiedmann, M. L., and Trumpler, P. R., 1946, "Thermal Accommodation Coefficients," *Trans. ASME,* Vol. 68, pp. 57–64.